Supplement of Ocean Sci., 21, 2149–2167, 2025
https://doi.org/10.5194/os-21-2149-2025-supplement

Ocean Science Open Access EGU

Supplement of

Assessment of ocean bottom pressure variations in CMIP6 HighResMIP simulations

Le Liu et al.

Correspondence to: Le Liu (le.liu@igg.uni-bonn.de)

S1 Full-depth eddy kinetic energy

At a given location, the vertically integrated (i.e., full-depth) eddy kinetic energy, as plotted in Fig. 7 in the main text, is $\rho_0 \int_{-H}^{0} \overline{\mathrm{EKE}\,(z)}\mathrm{d}z$ (Ni et al., 2023). Here, all auxiliary variables (ρ, z, H) are as defined near Eq. (1) in the main paper and $\overline{\mathrm{EKE}\,(z)}$ represents the time-mean eddy kinetic energy (EKE) at height z in the water column. The temporal average, indicated by the overbar, is taken over 20 years (1980–1999 or 2030–2049) of monthly EKE estimates

$$\mathrm{EKE}\,(z) = \frac{1}{2}\left(u(z)'^2 + v(z)'^2\right) \,. \tag{S1}$$

To evaluate Eq. (S1), we use each model's zonal (u) and meridional (v) velocity output and compute anomalies (u', v') with respect to the mean velocity components ($\overline{u}$, $\overline{v}$). Low-frequency or stationary changes in the ocean state, which are typically excluded in EKE calculations (e.g., Beech et al., 2022), are therefore part of the velocity anomalies. This processing choice is consistent with our elaborations in Sect. 3.6 in the main text, where we analyze and interpret p_b variability across all resolved frequencies.

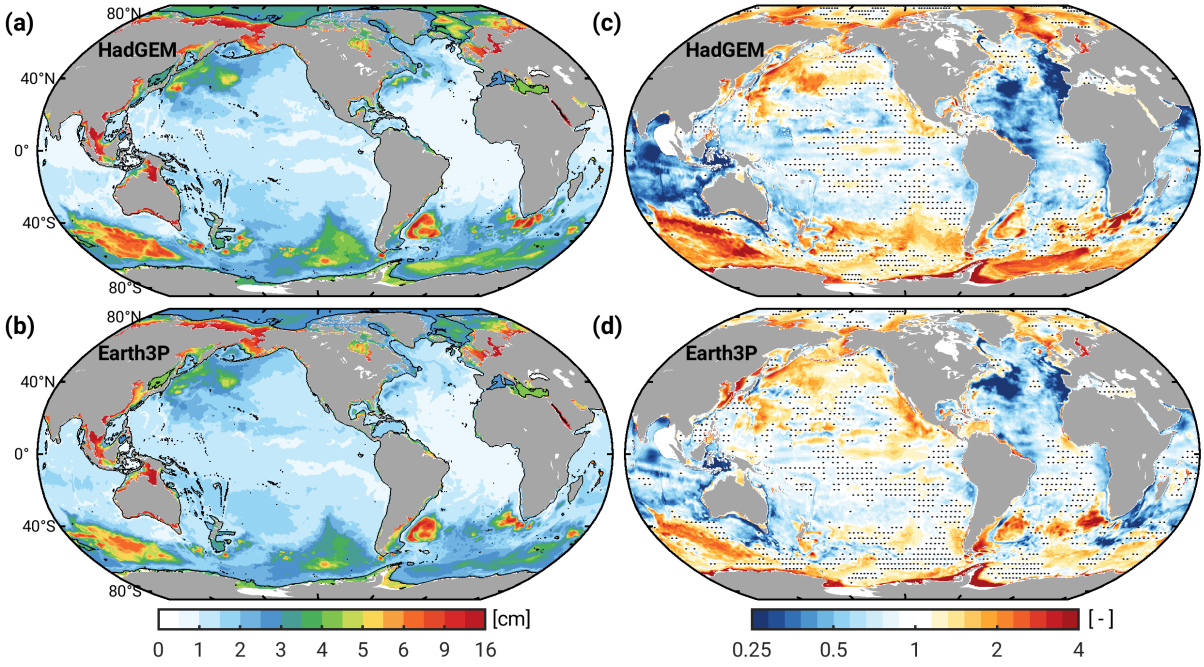

Figure S1. Similar to Fig. 2 in the main text but for CMIP6-HR 'pbo' output instead of inferred bottom pressure anomalies (see Sect. 2.2). Plots on the left show the RMS (cm) of p_b time series from HadGEM and Earth3P, computed as median of the RMS distribution over 1980–2014. Plots on the right show the variance ratio relative to the p_b variance from GRACE-DS. Stippling marks $3^\circ \times 3^\circ$ cells where the RMS of GRACE-DS is within the 10th–90th percentile range of the model RMS for at least a third of the contained 1/4° grid points.

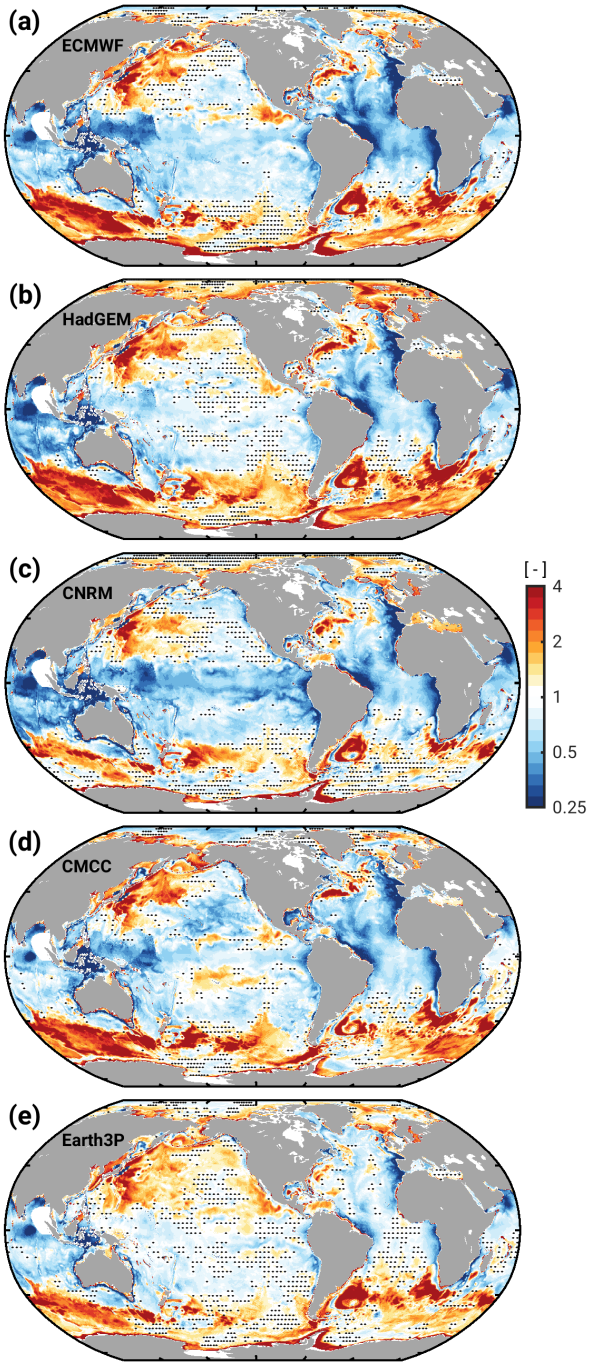

Figure S2. Variance ratios of the full CMIP6-HR p_b time series as in the right column of Fig. 2 in the main text, but with CSR mascons chosen as reference data. Stippling marks $3^\circ \times 3^\circ$ cells where the temporal RMS of the CSR fields is within the 10th–90th percentile range of the model RMS for at least a third of the contained $1/4^\circ$ grid points.

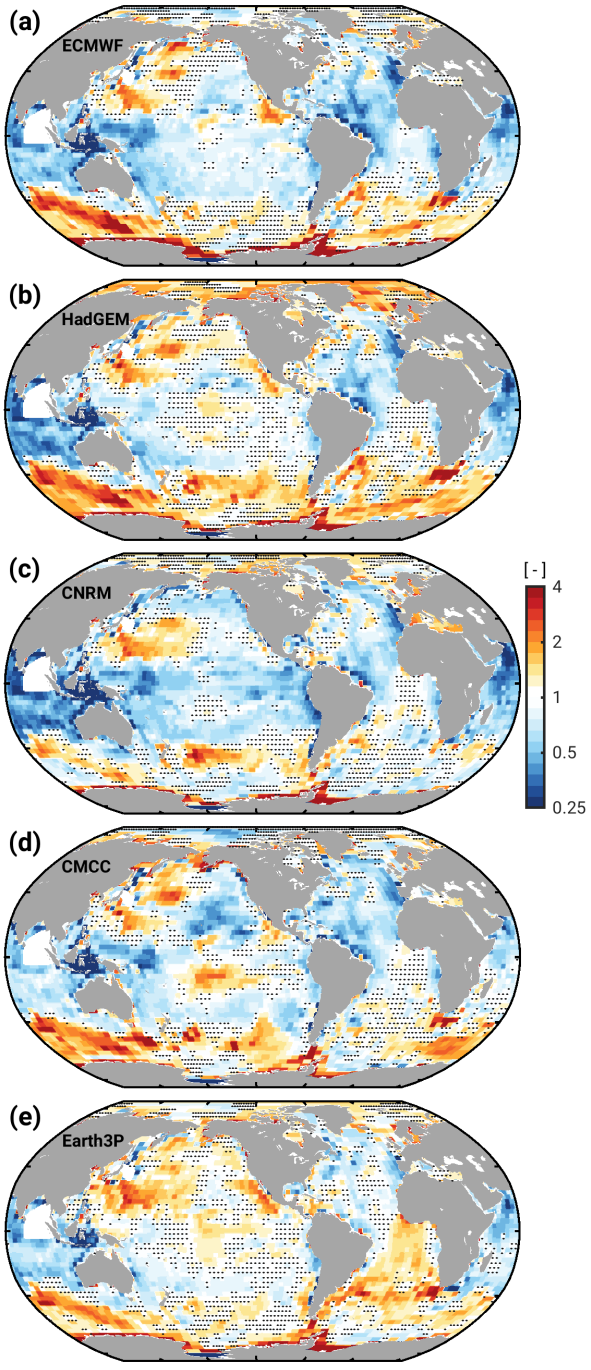

Figure S3. As in Supplementary Fig. S2, but with JPL mascons chosen as reference data and the model p_b fields averaged to the coarse JPL grid. Stippling marks $3^\circ \times 3^\circ$ cells where the temporal RMS of the JPL fields is within the 10th–90th percentile range of the model RMS. Large parts of the Andaman Sea and Bay of Bengal are affected by seismic signals in the JPL data and are therefore excluded from the plots (white mask). Note the visual differences with Supplementary Fig. S2 in the Atlantic, indicating comparatively higher variance in the JPL p_b data than in CSR.

Table S1. Global median variance ratios, $\overline{R}$, of the CMIP6-HR models relative to the CSR-based p_b variance[a]

Model Name	GRACE-DS, deep		GRACE-DS, shelf	
	RMS $>$ 3 cm	RMS $\leq$ 3 cm	$\lvert\phi\rvert > 60°$	$\lvert\phi\rvert \leq 60°$
ECMWF	2.20	0.76	1.38	1.19
HadGEM	1.87	0.88	2.07	1.40
CNRM	1.41	0.78	1.48	1.02
CMCC	2.35	0.76	1.44	1.30
Earth3P	1.78	0.95	1.57	1.40

[a] Global median values of R, split up into four regions as in Table 2 in the main text, but using the CSR mascons as reference data (see Supplementary Fig. S2). The Andaman Sea p_b anomaly in the CSR solution does not contribute to the comparison. All statistics pertain to the full (i.e., unfiltered) time series.

Table S2. Global median variance ratios, $\overline{R}$, of the CMIP6-HR models relative to the JPL-based p_b variance[a]

Model Name	GRACE-DS, deep		GRACE-DS, shelf	
	RMS $>$ 3 cm	RMS $\leq$ 3 cm	$\lvert\phi\rvert > 60°$	$\lvert\phi\rvert \leq 60°$
ECMWF	1.61	0.83	1.16	0.88
HadGEM	1.80	0.97	1.78	1.04
CNRM	1.18	0.82	1.22	0.77
CMCC	1.73	0.83	1.22	1.95
Earth3P	1.33	1.04	1.32	1.02

[a] Global median values of R, split up into four regions as in Table 2 in the main text, but using the JPL mascons as reference data (see Supplementary Fig. S3). The Andaman Sea/Bay of Bengal p_b anomaly in the JPL solution does not contribute to the comparison. All statistics pertain to the full (i.e., unfiltered) time series.

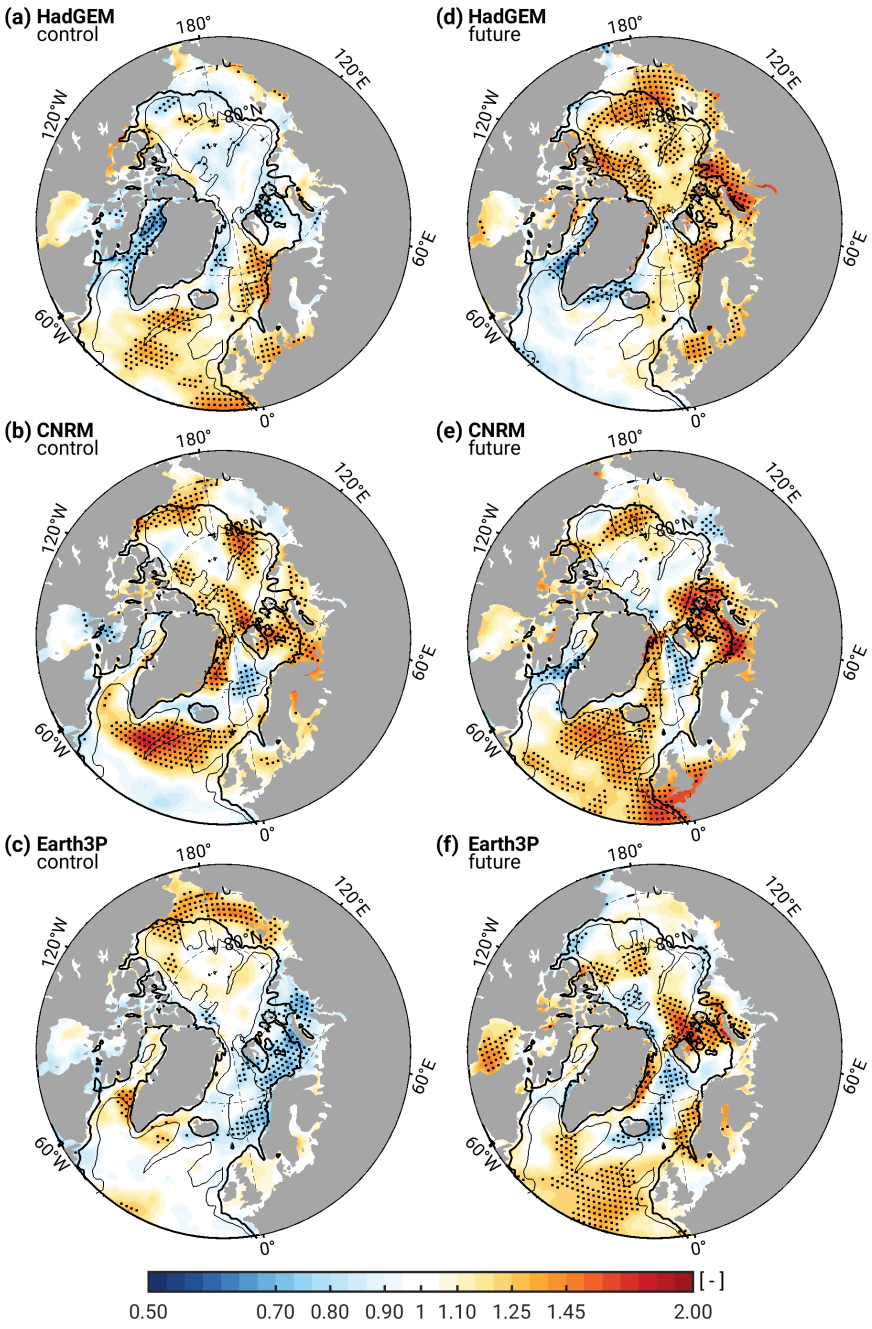

Figure S4. Variance ratios for near-surface wind speeds over the Arctic Ocean and neighboring seas, computed for the time period 2030–2049 relative to 1980–1999. Ratios are shown for HadGEM (top row), CNRM (middle row), and Earth3P (bottom row). Left panels (a–c) present the variance ratios from each model's control simulation, whereas the right panels (d–f) show the ratios formed from the scenario and historical simulations. Stipples indicate 1° equal-area cells where the variance ratio is significantly different from unity at 90% confidence for at least a third of the contained 1° grid points. The 200-m and 2000-m isobaths are shown as thick and thin black contours, respectively.

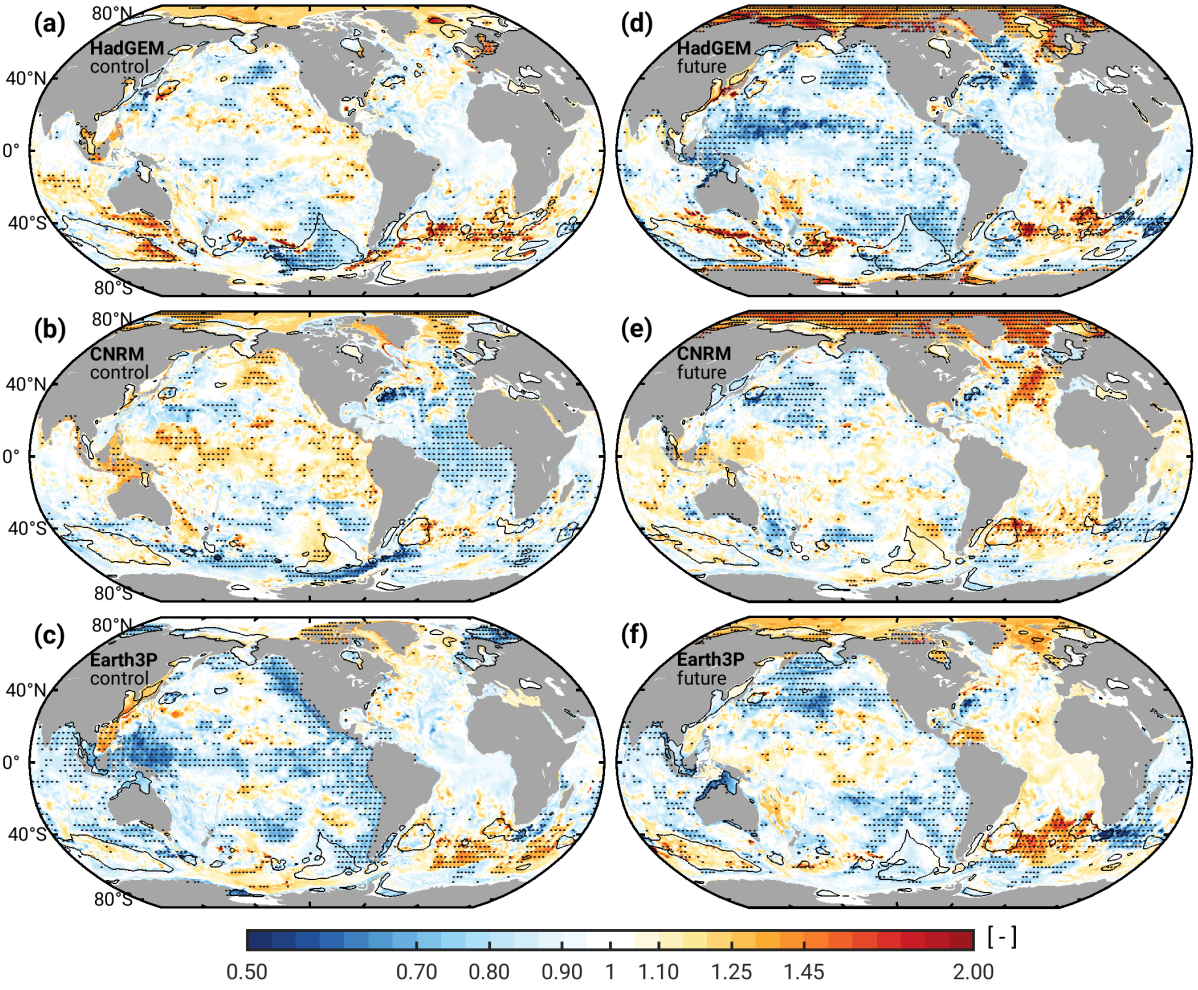

Figure S5. Dimensionless variance ratios as in Fig. 5 of the main text but with the p_b time series restricted to non-seasonal periods. Black contours encase areas where the non-seasonal RMS of each model exceeds 3 cm (smoothing to 200 km length scales applied).

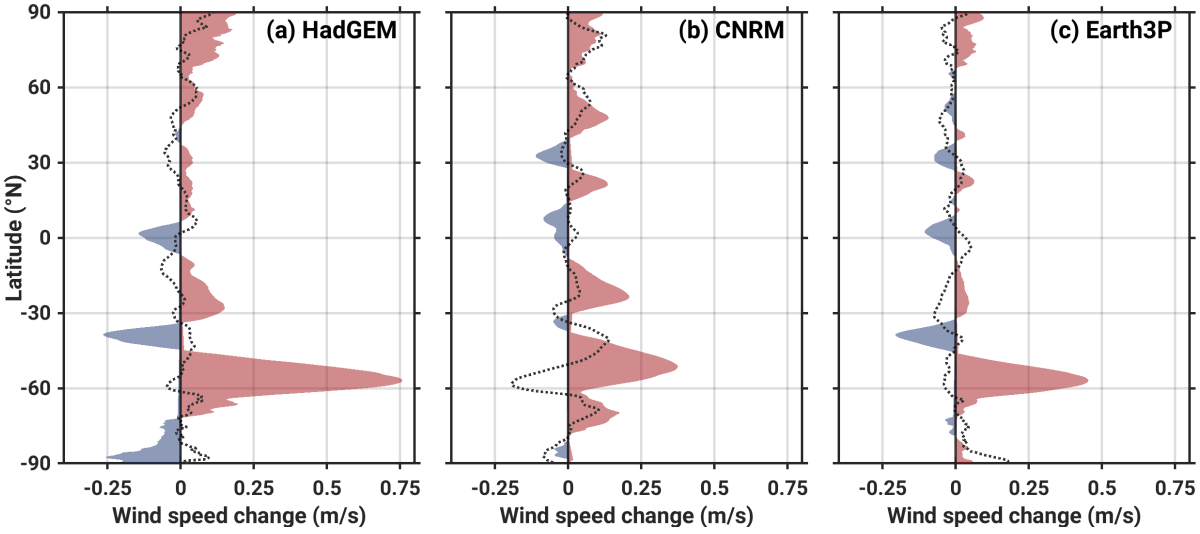

Figure S6. Change in zonally averaged global surface wind speed by 2030–2049 relative to 1980–1999 from the (a) HadGEM, (b) CNRM, and (c) Earth3P simulations (unit is m s^{-1}, land areas are included). Colored meridional profiles show the results from the scenario and historical runs, while the black dotted line indicates the corresponding profile from the control run.

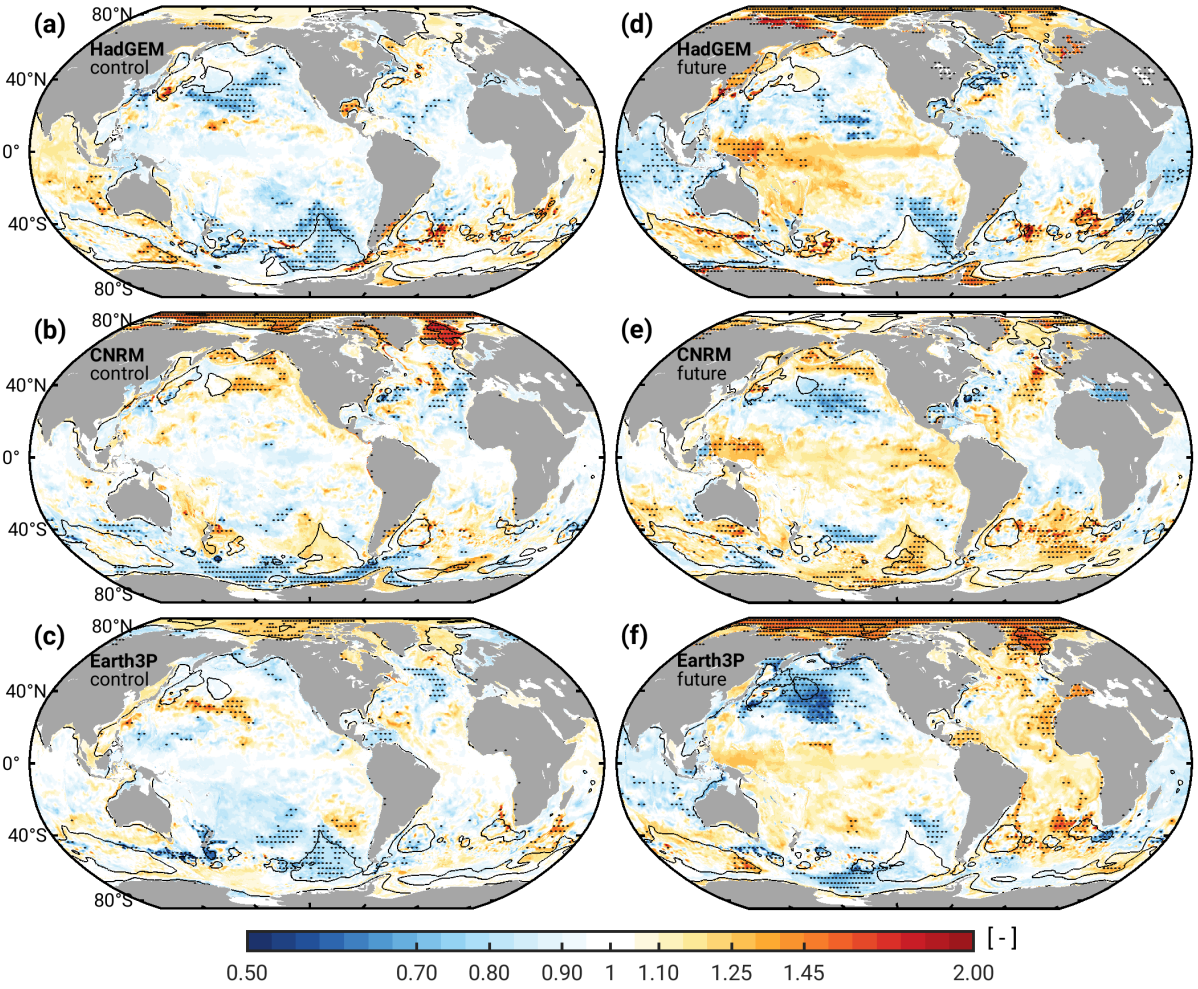

Figure S7. Dimensionless variance ratios for full p_b time series as in Fig. 5 of the main text but with a baseline period of 1995–2014 instead of 1980–1999.

Table S3. Global median variance ratios, $\overline{R}$, as in Table 1 of the main text but with the CMIP6-HR time series restricted to 2002–2014

Model Name	GRACE-DS, deep		GRACE-DS, shelf		BPRs[b]
	RMS $>$ 3 cm	RMS $\leq$ 3 cm	$\lvert\phi\rvert > 60°$	$\lvert\phi\rvert \leq 60°$	
ECMWF	1.54 (1.45)	0.74 (0.71)	1.19 (1.32)	0.70 (0.64)	1.03 (0.57)
HadGEM	1.61 (1.67)	0.88 (0.82)	1.70 (1.60)	0.86 (0.77)	1.05 (0.61)
CNRM	1.18 (1.19)	0.73 (0.67)	1.18 (1.19)	0.61 (0.55)	0.80 (0.49)
CMCC	1.84 (1.57)	0.80 (0.61)	1.24 (1.25)	0.74 (0.59)	0.79 (0.51)
Earth3P	1.38 (1.43)	0.95 (0.74)	1.23 (1.29)	0.86 (0.71)	1.33 (0.67)

References

Beech, N., Rackow, T., Semmler, T., Danilov, S., Wang, Q., and Jung, T.: Long-term evolution of ocean eddy activity in a warming world, Nat. Clim. Change, 12, 910–917, https://doi.org/10.1038/s41558-022-01478-3, 2022.

Ni, Q., Zhai, X., LaCasce, J. H., Chen, D., and Marshall, D. P.: Full-depth eddy kinetic energy in the global ocean estimated from altimeter and Argo observations, Geophys. Res. Lett., 50, e2023GL103 114, https://doi.org/10.1029/2023GL103114, 2023.